Spectroscopic and Structural Characterization of Chlorine Loading Effects on Mo/Si:Ti Catalysts in Oxidative Dehydrogenation of Ethane

Chang Liu and Umit S. Ozkan*

Department of Chemical Engineering, The Ohio State University, Columbus, Ohio 43210

Received: September 20, 2004; In Final Form: November 29, 2004

The structural changes induced in a silica−titania mixed-oxide support (1:1 molar ratio) by chlorine addition at different loading levels, their relation to the structural characteristics of supported MoO_x species over the support, and their correlation with ethane oxidative dehydrogenation (ODH) activity have been examined. The molybdenum and chlorine precursors are incorporated into the Si/Ti support network as it forms during gelation by using a "one-pot" modified sol−gel/coprecipitation technique. In situ X-ray diffraction during calcination shows the Si/Ti 1:1 mixed-oxide support is in a state of nanodispersed anatase titania over amorphous silica. With the addition of molybdenum and chlorine modifier, this anatase feature becomes more pronounced, indicating a decreased dispersion of titania. The effective titania surface area on the chlorine-doped Si:Ti support obtained from 2-propanol temperature-programmed reaction supports this observation. Raman spectra of dehydrated samples point to an enhanced interaction of MoO_x species with silica at the expense of titania. X-ray photoelectron spectroscopic results show that, without forming a molybdenum chloride, the presence of chlorine significantly alters the relative surface concentration of Si vs Ti, the electronic structure of the surface MoO_x species, and the oxygen environment around supported MoO_x species in the Si/Ti network. Secondary ion mass spectrometry detected the existence of SiCl fragments from the mass spectra, which provides molecular insight into the location of chlorine in Mo/Si:Ti catalysts. The observed increase in ethane ODH selectivity with chlorine modification may be ascribed to the MoO_x species sharing more complex ligands with silica and titania with the indirect participation of chlorine. Steady-state isotopic transient kinetic analysis (SSITKA) is used to to examine the oxygen insertion and exchange mechanisms. The catalysts show very little oxygen exchange with the gas phase in the absence of a reaction medium. During the steady-state ODH reaction, lattice oxygen appears to be the primary source of oxygen in the formation of water and CO_2.

Introduction

The selective partial oxidation and oxidative dehydrogenation (ODH) of lower alkanes have attracted significance research interest because commercialization can lead to utilization of relatively inexpensive and abundant alkane resources from natural gas and petroleum fractions as a feedstock.[1−5] In particular, the production of ethylene through ethane ODH has been extensively studied since the 1990s, given its high demand for the production of polyethylene, ethylene dichloride, ethylene oxide, and ethylbenzene.[6,7] Thus far, there is no industrial process of ethane ODH because the ethylene yield achievable is still not commercially competitive.[8] The balance between activity and selectivity control is still a major challenge because ODH of ethane to ethylene occurs via parallel and sequential oxidation steps in which ethylene is the primary ODH product, whereas CO_x can form via either direct combustion of ethane or secondary combustion of ethylene.[9−12]

While addition of chlorine into the feed stream has achieved higher ethylene yields at higher temperatures, this is not a practical solution due to environmental issues associated with use of halides in the feed.[1,8] Although it is generally accepted that, at higher temperatures, the reaction follows a homogeneous gas-phase mechanism in which ethane ODH occurs through the formation of ethyl radicals that react in the gas phase to form ethylene,[1,2] the surface mechanism at lower temperatures still needs further elucidation due to competitive steps that exist between the selective mechanism, normally a Mars van Krevelen redox cycle,[13] and the nonselective steps, including oxygen insertion, activated from the gas phase or from the lattice oxide, into ethane or ethylene, to form carbon oxides.[14−22] An optimal balance between redox potential, adsorption/desorption characteristics, and oxygen mobility is essential for an optimum combination of activity and selectivity. Selective and active catalysts are likely to possess a certain degree of structural complexity to serve this purpose.[23−25]

Molybdenum catalysts supported over Si:Ti oxides were shown to be both active and selective for ODH of light alkanes in our previous work.[26−30] Several molybdenum species may coexist in the form of Mo═O, Mo−O−Mo, Mo−O−Si, or Mo−O−Ti structures, and the complex functionality could be achieved through multiple oxidation states and coordination environments of Mo and varying support interactions with Si vs Ti.[25] The structural characteristics over Mo/Si:Ti 1:1 catalysts and the structural effects induced by alkali metal promoters showed that the presence of potassium significantly alters the electronic structure of surface MoO_x domains and octahedral MoO_x structures become more distorted at low alkali metal levels. Concurrent with this observation is a broad maximum in activity and selectivity for propane ODH with the alkali metal promoter loading level.[28] This strong promotional effect on propane ODH does not, however, reproduce itself on ethane

* To whom correspondence should be addressed. Phone: (614) 292-6623. Fax: (614) 292-9615. E-mail: ozkan.1@osu.edu.

10.1021/jp045726m CCC: $30.25
Published on Web 01/26/2005

TABLE 1: Surface Area, Pore Volume, and Pore Size of Sol−Gel Catalysts

catalyst	surf. area (m^2/g)	pore vol. (cm^3/g)	pore size (nm)
10% Mo/Si:Ti = 1:1	133	0.17	3.8
Cl/Mo = 0.1	141	0.19	4.0
Cl/Mo = 0.3	194	0.22	3.9
Cl/Mo = 1.0	196	0.25	3.9
Cl/Mo = 2.0	230	0.28	3.8

ODH, and the latter seems better served by chlorine promotion.[30] There have been previous reports in the literature citing the effect of chlorine on surface properties by creating active centers, improving dispersion, stabilizing chemical phases, adjusting reducibility, and modifying lattice oxygen mobility over different catalytic systems.[31−35] We have previously reported the redox and adsorption/desorption properties of Cl-modified Mo/Si:Ti.[36] In this article, we address the structural effects induced by chlorine addition for Mo/Si:Ti 1:1 catalyst and its relevance to ethane ODH activity.

Experimental Section

Catalyst Preparation. Catalysts were prepared using a "one-pot" sol−gel/coprecipitation technique that was described previously.[36,37] The technique distributes the active metal precursors throughout the Si:Ti support network as it forms during gelation. Tetraethyl orthosilicate (TEOS) (Aldrich) and titanium(IV) isopropoxide (TIPO) (Aldrich) were used for preparing the silica−titania mixed-oxide supports. Ammonium heptamolydate (AHM) (Mallinckrodt) and NH_4Cl (Mallinckrodt) were used as precursors for molybdenum and chlorine, respectively. A mixture of ethanol and isopropyl alcohol with a volume ratio of 1:1 was used as the solvent. Synthesized catalysts are listed in Table 1 with the Cl/Mo ratio ranging from 0 to 2 at a constant (10 wt %) loading of Mo and a Si/Ti molar ratio of 1:1. The Mo loading level corresponds to a Mo/Si molar ratio of 0.162.

Catalyst Characterization. BET surface area measurements and nitrogen adsorption−desorption isotherms were recorded using a Micrometrics ASAP 2010 instrument. Nitrogen was used as an adsorbate at liquid nitrogen temperature (77 K). The samples were degassed at 200 °C for 8 h before surface area measurements. The pore volume and pore size distribution were calculated from the desorption isotherm by using the BJH method.

In situ X-ray diffraction patterns during calcination were obtained on a Bruker D8 Advance diffractometer operated at 2 kW with Cu Kα radiation as the X-ray source. The diffractometer is equipped with an Anton-Paar HTK1200 temperature stage that is capable of bringing samples in contact with flowing gas at any desired temperature from ambient to 1200 K. The diffraction patterns were recorded in the 2θ range from 20° to 90°, and the temperature was raised from 50 to 650 °C at 50 °C intervals.

Temperature-programmed reaction after 2-propanol adsorption was performed on chlorine-doped Si:Ti supports corresponding to Cl/Si ratios of 0, 0.016, and 0.160 using a laboratory-made gas flow system described elsewhere.[38] Catalyst samples (with equal surface area of 27 m^2) were placed in a 1/4-in.-i.d. U-tube quartz reactor, pretreated under oxygen flow at 550 °C for 30 min followed by cooling to 80 °C under helium, and finally flushed with helium for 1 h following 1 h of 2-propanol adsorption at 80 °C. 2-Propanol was introduced by flowing helium through a diffusion tube containing 2-propanol heated at 80 °C. Species desorbing under a helium carrier gas were monitored by a mass spectrometer (HP5890 GC−MS). The mass spectrometer was equipped with a quadrupole mass analyzer that allows tracking of up to 20 mass-to-charge ratios (m/e) simultaneously in the selected ion mode, and the desorption peak from propylene was used for the calculation of effective titania surface area. The propylene peak was calibrated by pulsing pure propylene from a sample loop with 0.2 cm^3 volume to the GC−MS. The amount of propylene evolved from bulk TiO_2 prepared by sol−gel method and its BET surface area were used to calculate the effective titania surface area. The temperature program was as follows: 10 min at 80 °C, 10 °C/min ramp rate to 600 °C, and holding at 600 °C for 10 min.

Raman spectra were recorded with a Kaiser Raman spectrometer using a 514.5 nm laser. Spectra were taken in the range of 300−1500 cm^{-1} in the 180° backscattering mode with a CCD detector. Spectra were averaged over 10 scans with 10 s integration time for each scan. Naphthalene was used as a standard to calibrate the instrument. Raman spectra under dehydrated conditions were acquired using a quartz in situ flow cell that is capable of flowing gas through the catalyst at high temperature. A portion of the prepared catalyst was recalcined at 550 °C for 30 min under pure oxygen and transferred into the Raman cell. Additional dehydration was performed at 350 °C for 30 min under a flow of 10% oxygen/helium, after which the cell was sealed at both ends. Spectra were taken under a 10% oxygen/helium atmosphere at room temperature.

X-ray photoelectron spectroscopy of catalysts was performed with a Kratos Ultra Axis spectrometer using Al Kα (1486.3 eV) radiation operated at 14 kV. Catalyst samples were recalcined at 550 °C for 30 min under pure oxygen before XPS analysis. The XPS spectra of each element were averaged over 10 scans. Spectra were corrected using the C 1s signal located at 284.6 eV, and surface concentrations were determined using instrumental atomic sensitivity factors.

Secondary ion mass spectrometry (SIMS) of the studied catalysts was performed using a PHI THRIFT 3 spectrometer operating under static limit. This time-of-flight SIMS has high mass capability with mass spectra ranging from 1 to >10 000 of m/e ratio and high mass resolution for separation of nearly identical masses. The catalyst samples were hard-pressed onto an indium disk and mounted on a copper support. Cs^+ and O_2^+ beams were used for negative and positive SIMS, respectively, to sputter a spot area of 500 × 500 μm. Ga^+ beam was used as the analysis beam, and each mass spectrum was the accumulation of a spot area of 200 × 200 μm. The analysis of mass spectra and assignment of mass fragments were performed using reference patterns from a database provided by Science Instrument Services Inc.

Oxidative Dehydrogenation of Ethane. Cl/Mo catalysts were tested for the ethane ODH reaction in a fixed-bed quartz reactor operating at ambient pressure. Catalyst samples were held in place by a quartz frit, and the total flow rate was maintained at 25 cm^3/min with a feed composition of ethane/oxygen/nitrogen ratio of 10/5/85, which is outside the flammability limits of ethane/ethylene−oxygen−nitrogen mixtures. The major reaction products were ethylene, methane, carbon dioxide, carbon monoxide, and water, which were separated and analyzed online using a HP 5890 Series II gas chromatograph containing FID and TCD detectors. Separations were performed using three columns: (1) Hayesep D (8 ft × 1/8 in.) for hydrocarbons and partially oxygenated hydrocarbons, (2) Porapak Q (6 ft × 1/8 in.), and (3) molecular sieve 5 Å (6 ft × 1/8 in.) for N_2, O_2, CO, CO_2, and H_2O. To ensure that any surface-assisted gas-phase reactions in the presence of a catalyst

were minimized, the dead volume of the quartz reactor was packed with quartz wool and/or ceramic beads. Reaction data were taken after steady state was reached, and the product distribution maintained a carbon balance of 100% (±5%) for all runs.

Steady-State Isotopic Transient Kinetic Analysis (SSITKA). Isotopic exchange flow experiments using $^{18}O_2$ with and without the presence of steady-state reaction of ethane ODH were performed with a laboratory-made gas flow system by establishing two gas-feed streams and utilizing a four-port Valco valve to switch between unlabeled and labeled gas streams. Catalyst samples (100 mg) were placed in a 1/4-in.-i.d. U-tube quartz reactor and pretreated under oxygen ($^{16}O_2$) flow at 600 °C for 30 min. For isotopic oxygen switch without reactions, a mixture of 10% $^{16}O_2$ in helium with a small amount of argon present (~1%) was passed over the samples and allowed to stabilize. After steady mass spectrometer signals were obtained, the flow was switched to that containing 10% $^{18}O_2$ in helium and the exchange was carried out for 15 min at 600 °C. For isotopic oxygen switch with reactions, the first stream contained 5% C_2H_6, 2.5% $^{16}O_2$, 91.5% He, and 1% argon, and the second mixture contained 5% C_2H_6, 2.5% $^{18}O_2$, and 92.5% He. The first reaction mixture was introduced at the total flow rate of 25 cm^3/min and reaction was carried out in the U-tube reactor until steady state was established at 600 °C. The flow was subsequently switched to the second stream containing corresponding labeled isotopes without perturbing the steady state, and the exchange was carried out for 15 min at 600 °C. All the oxygen-containing species and argon were monitored by a mass spectrometer (Shimadzu GCMS-QP5050A) under helium carrier gas with the capability to track up to 64 mass-to-charge ratios (*m*/*e*) simultaneously in the selected ion mode. The normalized concentration of each isotope for a given species was calculated by dividing the signal for that isotope by the sum of the signals for all the isotopes of that species.

Results and Discussion

Surface Area and Pore Size. Comparing the surface areas of the prepared catalysts (Table 1), it can be seen that the incorporation of chlorine into Mo/Si:Ti catalyst increases the surface area at successive levels up to Cl/Mo = 2.0. The higher surface area could allow a better dispersion of molybdena species and is one of the motivations for using a sol−gel preparation. The nitrogen adsorption−desorption isotherm of the catalysts indicated a micro- to mesoporous structure. The pore volume and pore size distribution were calculated using the desorption isotherm. It can be seen that there is a steady increase of average pore volume with chlorine loading amount, while average pore size is relatively constant for all chlorine-containing catalysts.

In Situ X-ray Diffraction. In situ XRD patterns taken during the temperature programmed calcination process are shown in Figure 1 for two catalyst samples, with and without Cl loading. Neither precursor shows any crystallinity until a calcination temperature of 450 °C is reached. Silica−titania mixed oxides are known to exhibit a small particulate anatase structure supported over amorphous silica.[39] Above 450 °C, a broad peak appears and becomes more intense at higher temperatures, which is assigned to the most intense diffraction line from anatase structure. For the Cl-doped catalyst, this feature becomes even sharper, especially at higher calcination temperatures. It is generally accepted that, on silica−titania mixed oxide, titania species are dispersed mainly by interaction with silica. The results here show that, with the introduction of low levels of chlorine promoter, the dispersion of titania decreases as does the interaction of titania species with silica. In particular, at higher calcination temperatures, evident separation of an anatase titania phase is apparent. It is conceivable that the addition of chlorine favors a stronger interaction of silica with molybdenum at the expense of titania. Molybdena species are believed to be finely dispersed because no MoO_3 diffraction lines were observed on both Mo-only and chlorine-addition catalysts. However, the possibility that MoO_3 exists as a microcrystalline material below the XRD detection limit cannot be excluded.

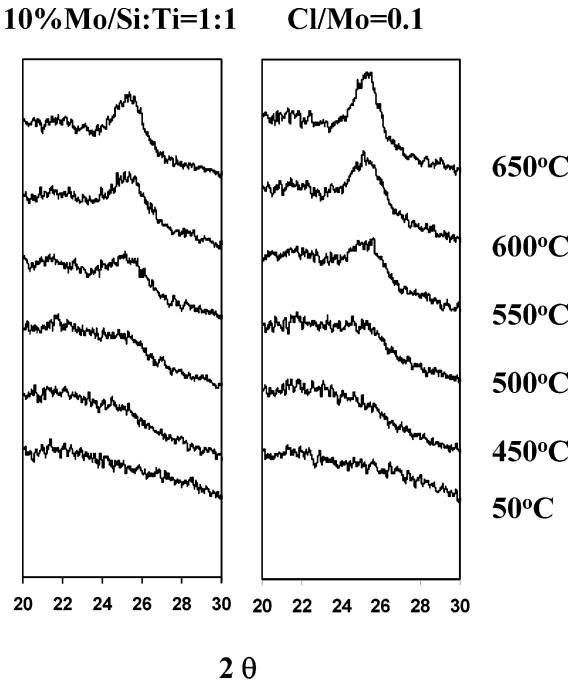

Figure 1. In situ X-ray diffraction patterns during calcination for (Cl/Mo)/Si:Ti catalysts.

2-Propanol Temperature-Programmed Reaction (TPRxn). The temperature-programmed reaction of 2-propanol has been used previously to measure the titania surface area of mixed oxides of titania and silica.[40−43] It was proposed that the dehydration of the adsorbed 2-propanol on the titanyl and silanol groups takes place at two distinct temperatures and the effective titania surface area can be measured through quantification of the evolved propylene over the titanyl groups via mass spectrometry.[42,43] However, this technique cannot be used in the presence of an active metal as reported by Swain et al., who used 2-propanol TPRxn to determine the effective titania surface area in silica−titania mixed oxides prior to vanadium impregnation.[44] Vanadia is known to react with alcohols to form acetone and to preferentially adsorb onto TiO_2, thereby blocking dehydration reaction sites. Since selective oxidation functionality over molybdenum- and vanadium-containing catalysts are similar, it can be expected that, when supported on a binary oxide, molybdena species will exhibit behavior similar to those of vanadia species.[45] This was confirmed by a test on a molybdenum-containing Si:Ti support, where multiple desorption features were observed making the peak assignment and deconvolution quite complex, if not totally impossible. Therefore, the data obtained from Mo-containing samples were not included in the analysis and the technique was used to examine the effect of Cl addition on the mixed-oxide support without any metal addition.

All chlorine-doped Si:Ti supports with Cl/Si ratios of 0, 0.016, and 0.16 showed similar desorption patterns after 2-propanol adsorption and analysis of the desorbed species showed the

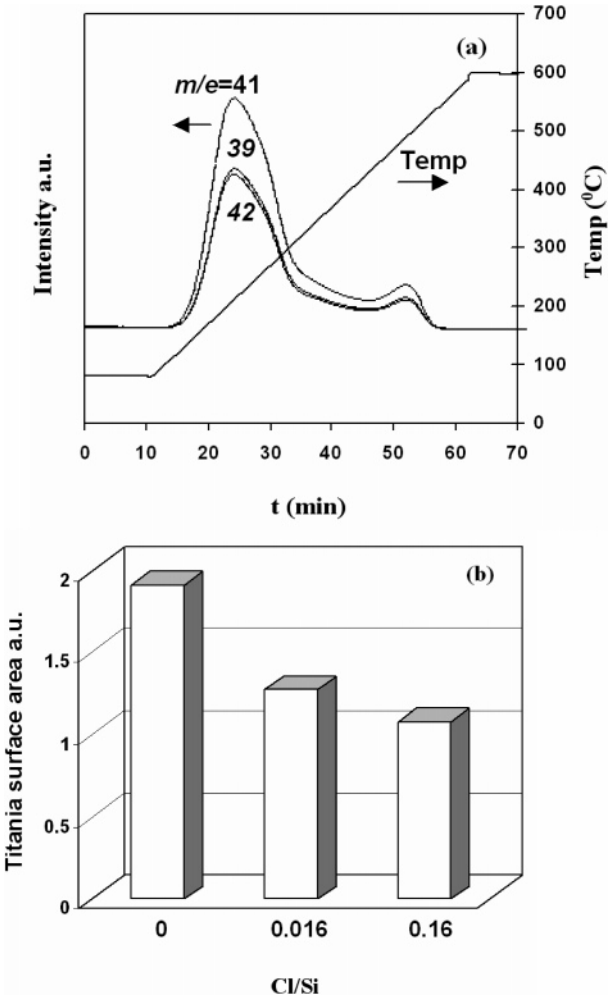

Figure 2. 2-Propanol TPRxn of Cl-doped Si:Ti support: (a) propylene desorption profiles; (b) variation of titania surface area of the support with Cl addition.

primary species of 2-propanol, propylene, water, and trace amounts of acetone and ethyl ether desorbing from the surface. The propylene desorption profile for Si:Ti support is presented in Figure 2a. It can be seen that there are two well-resolved desorption features located at different temperature ranges. When the results were compared with those of the bulk TiO_2, where only one desorption feature was observed, it was seen to coincide with the lower temperature feature for the mixed Si:Ti support for both chlorine-free and Cl-containing samples. Thus, this lower temperature desorption feature was assigned to 2-propanol dehydration on the titanyl groups and was used to determine how much of the surface is covered by titania. The effective titania surface area calculated by following the methodology reported in the literature[44] was plotted in Figure 2b as a function of Cl loading, which shows that the exposed titania surface area decreases substantially with successive levels of chlorine loading. Although the results obtained may not necessarily represent the absolute titania surface area, they nevertheless represent a trend. Since the catalyst charge for all runs was based on the same total surface area, the change in the measured exposed titania surface area represents a change in the extent of dispersion and segregation of titania in the Si:Ti network. Although the effect of Cl on the support structure after introducing molybdenum might not be exactly the same as Mo-free Si:Ti support, its effect on the dispersion of titania in the Si:Ti matrix is unambiguous. When compared with in situ XRD calcination results, it can be seen that addition of Cl changes the Si−Ti interaction even in the presence of the active metal, i.e., Mo.

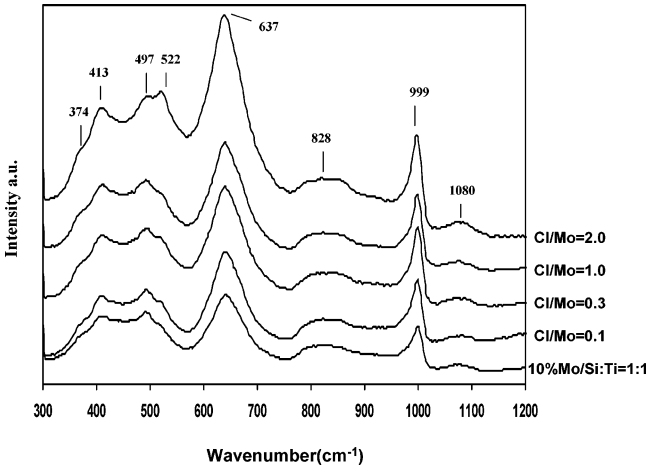

Figure 3. Raman spectra of (Cl/Mo)/Si:Ti catalysts under dehydrated conditions.

Raman Spectroscopy. The Raman spectra of "dehydrated" samples are shown in Figure 3. One evident feature of the spectra is that there are no bands associated with Mo−O−Mo stretching vibrations around 820 cm^{-1}, which would signal the presence of crystalline MoO_3. This is rather expected since the sol−gel technique disperses molybdenum species throughout the Si:Ti network. The bands associated with anatase titania are shifted to lower wavenumbers compared to those of pure anatase[46] and appear at 637, 497, and 413 cm^{-1}. With the introduction of chlorine at successive levels, these bands grow in intensity and the features presented as shoulders located at 522 and 374 cm^{-1} become more intense, indicating the effect of chlorine on the titania domains. A broad band was observed in the range of 750−950 cm^{-1}. There could exist multiple contributions for this feature, including antisymmetric stretching of Mo−O−Mo bonds,[47] symmetric mode of Si−O−Si stretching,[48] and surface-coordinated Mo−O−Mo vibrations from polymolybdate structures.[30] The feature located at 1080 cm^{-1} is indicative of Ti−O−Si bonds,[49,50] and is perturbed by or overlapped with the asymmetric Si−O−Si stretching vibration, which is located at 1050 cm^{-1} for pure silica.[51] The bands associated with isolated terminal Mo═O stretching vibrations are present in the 970−1005 cm^{-1} range, and the contributions to this band can come from molybdena species supported solely on silica or titania domains of the support, or from species sharing mixed support−O ligands.[47] Although there is a scarcity of data from the literature on Raman bands arising from surface supported molybdenum species over binary oxides of silica−titania under dehydrated conditions, Wachs[52,53] has summarized the Raman data of molybdena species supported over silica and titania individually under dehydrated conditions and stated that, depending on different preparation methods, terminal Mo═O bands of surface molybdena species supported over silica appear in the range of 975−990 cm^{-1} while for titania the band shifts to a higher range of 998−1001 cm^{-1}. It can be seen that the bands associated with terminal Mo═O stretching vibrations shift to lower wavenumbers with the addition of chlorine and the bands become less symmetrical. The data in the literature suggest that it is possible to interpret the Raman spectra of molybdena species supported over binary oxides to gain qualitative information as to whether molybdena species preferentially interacts with one of the oxide domains by incorporating different support−O ligands because the shifts in the Mo═O Raman frequency are related to changes in bond length[52] and

TABLE 2: Surface Concentrations of Mo, Si, and Ti Calculated from XPS Analysis

catalyst	Si (%)	Ti (%)	Mo (%)
as-prepared	46.25	46.25	7.5
10% Mo/Si:Ti = 1:1	50.99	40.30	8.7
Cl/Mo = 0.1	49.66	41.43	8.9
Cl/Mo = 0.1	53.24	38.26	8.5
Cl/Mo = 0.1	56.88	35.88	7.2
Cl/Mo = 0.1	60.31	34.29	5.4

TABLE 3: Mo $3d_{5/2}$ Binding Energy of Catalysts and Reference Compounds

Mo $3d_{5/2}$	BE (eV)
10% Mo/Si:Ti = 1:1	232.8
Cl/Mo = 0.1	232.9
Cl/Mo = 0.3	232.9
Cl/Mo = 2.0	233
$MoCl_4$	230.6
$MoCl_5$	231
MoO_3	232.6
Mo(V)/Al	231.5

TABLE 4: O 1s Binding Energy of Pure Oxides

O 1s	BE (eV)
SiO_2	533.8
TiO_2	529.2
MoO_3	531.6

could result from the change of interaction with the support. The Raman results here indicate that, with the incorporation of chlorine, molybdena species interact increasingly with silica at the expense of titania. Concurrent with this change is the observation of decreased titania dispersion.

X-ray Photoelectron Spectroscopy (XPS). To further study the nature of molybdena species over the silica−titania mixed-oxide support, X-ray photoelectron spectra were taken over chlorine-containing catalysts with Cl/Mo = 0−2.0. The surface concentrations, as determined by XPS, are presented in Table 2. When compared to the as-prepared values for the catalysts studied, there is a surface enrichment of Si at the expense of Ti even for Mo-only catalyst. Due to the difficulty of dispersing titania over silica, a lower Ti concentration relative to Si is commonly observed by XPS measurement for Si:Ti binary support prepared by different methods.[46,54] Another possibility as suggested in the literature is that the majority of Ti atoms may reside on the surface of inside channels or pores of silica, which can be out of the XPS detection range.[49] It is interesting to note that, with the introduction of chlorine at successive levels, this trend becomes more pronounced while the surface concentration of Mo is relatively constant, with the exception of Cl/Mo = 2.0, where a substantial decrease is observed. This suggests that without causing an evident change in the surface concentration of Mo, the addition of chlorine could decrease the interaction of Ti with Si and cause the segregation of a crystalline anatase phase from the Si:Ti network.

The Mo 3d regions of XPS are plotted in Figure 4, and the Mo $3d_{5/2}$ binding energies for catalysts with different Cl/Mo ratios were compared with the data from the literature in Table 3. All catalysts exhibit one broad linked doublet, indicative of molybdenum trioxide, corresponding to Mo $3d_{5/2}$ and $3d_{3/2}$ binding energies at 232.6 and 235.7 eV. With the addition of chlorine, both peaks are seen to shift to a higher binding energy range and the Mo 3d spectrum of Cl/Mo = 2.0 catalyst becomes much broader, showing some convoluted feature at a lower binding energy around 231.6 eV. This feature cannot be ascribed to molybdenum chloride since the Mo $3d_{5/2}$ binding energies for $MoCl_4$ and $MoCl_5$ have been reported to be located at

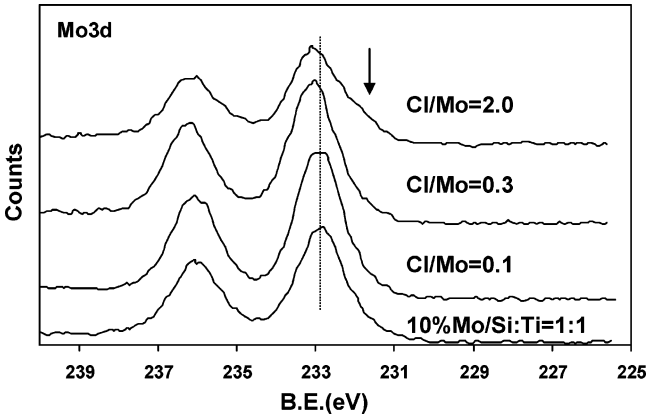

Figure 4. Mo 3d X-ray photoelectron spectra for (Cl/Mo)/Si:Ti catalysts.

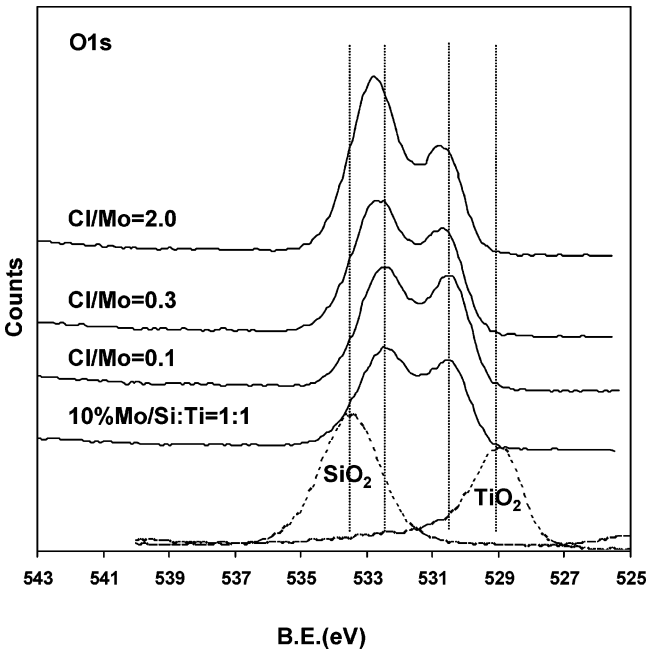

Figure 5. O 1s X-ray photoelectron spectra for (Cl/Mo)/Si:Ti catalysts and supports.

230.6−231 eV.[55−57] However, a reduced Mo(V) species was reported to have a binding energy between 231 and 231.5 eV on alumina-supported catalysts.[58−60] Therefore, it is conceivable that this extra feature comes from the electronic interaction of chlorine with surface molybdena species without forming a new molybdenum chloride compound. The chlorine addition seems to have the strongest influence on Cl/Mo = 2.0 catalyst, as seen from surface concentrations determined from XPS, where the amount of molybdenum species experienced the most pronounced decrease at Cl/Mo = 2.0 catalyst.

Additional XPS characterization was performed over the chlorine-containing catalysts including the O 1s, Si 2p, and Ti 2p regions. The O 1s spectrum is shown in Figure 5, and the results from pure SiO_2 and TiO_2 are also included for comparison purposes.[28] The relevant binding energy of O 1s is given in Table 4. It is evident that oxygen contributions come from not one, but a distribution of chemical environments including SiO_x, MoO_x, and TiO_x. With the addition of chlorine, the peak located at higher binding energy increases while the lower binding energy feature decreases, which might indicate the surface enrichment of Si relative to Ti, as already seen from surface concentration distribution. The Si 2p and Ti 2p XPS are shown in Figure 6. The Si 2p spectra of all samples appeared

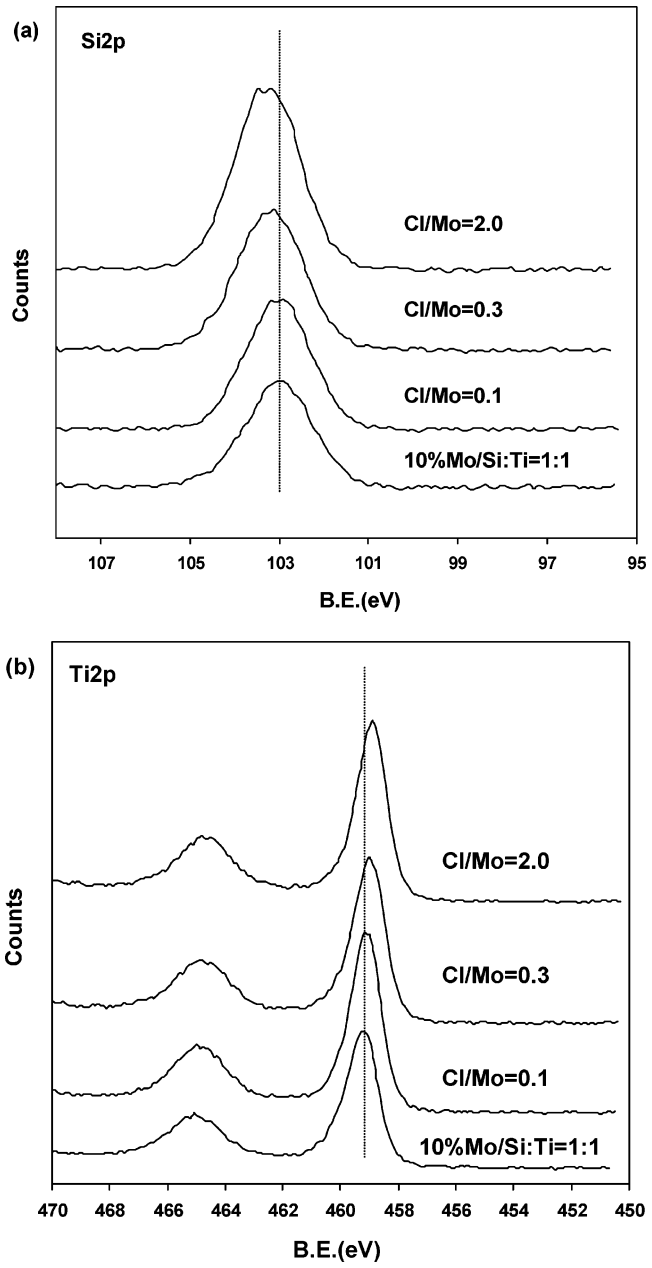

Figure 6. X-ray photoelectron spectra for (Cl/Mo)/Si:Ti catalysts: (a) Si 2p; (b) Ti 2p.

at higher binding energy compared with that of pure SiO_2 and exhibited a peak located around 103.2 eV. This peak shifts to higher binding energy with the Cl/Mo ratio, indicative of the effect chlorine has on silica domain. There have been reports in the literature where chlorine has been referred to as a "damaging precursor" when present on silica glasses and has been found to significantly distort silica glass networks.[61,62] The Ti 2p spectrum of Mo-only catalyst exhibited one linked doublet corresponding to Ti $2p_{3/2}$ and $2p_{1/2}$ binding energies at 459.1 and 464.9 eV, respectively, indicating that titania is closely interacting with silica and in a state of very small anatase domains.[63] With the addition of chlorine, the Ti 2p binding energy shifts to lower values, reaching 458.8 eV for Cl/Mo = 2.0. Since shifts in Ti 2p binding energies are indicative of changes in the dispersion of titania over silica,[26,28,59] it is concluded that the introduction of chlorine significantly alters the dispersion of titania over the silica matrix, which is in agreement with previous results.

Secondary Ion Mass Spectroscopy. Static secondary ion mass spectromety (S-SIMS) has been used extensively in recent years to determine the surface composition and properties of solid catalysts.[64,65] In particular, one application of S-SIMS is the characterization of the chemical form of chlorine-containing noble metals.[66,67] To further investigate the influence of chlorine on the interaction of surface molybdena species with Si:Ti support, SIMS analysis was performed in an effort to pinpoint the location of chlorine and to provide molecular insight with regard to its modification of the catalyst surface through chemical bonding. The negative SIMS mass spectra in the typical range of chlorine are presented in Figure 7 for catalysts with Cl/Mo = 0.3 and 1.0. The existence of chlorine at the catalyst surface was confirmed by a pair of peaks with *m*/*e* ratios of 35 and 37 whose integral intensity is proportional to the isotope abundance of chlorine corresponding to $^{35}Cl^-$ and $^{37}Cl^-$, respectively. Without having a reference material that has both structural and compositional similarity to our catalyst samples to ensure similar secondary ion yields, the absolute concentration of chlorine cannot be reliably determined. Since oxygen constitutes a matrix for mixed metal oxides and a negative SIMS image for $^{16}O_2^-$ was almost identical to that for total ions, the ion yield ratio of $^{35}Cl^-$ to $^{16}O_2^-$ was used to represent the relative concentration of chlorine. It can be seen that the intensity of $^{35}Cl^-$ and $^{37}Cl^-$ ions relative to $^{16}O_2^-$ is higher at higher chlorine loading.

The SIMS method not only gives the relative concentration of chlorine, but also indicates the structural groups containing chlorine atoms. The positive SIMS mass spectra for Mo-only and Cl-containing catalysts were compared in the vicinity of TiO^+ mass fragment. The results are given in Figure 8, where the mass abundances of different ions from *m*/*e* = 62 to 67 are presented relative to the most abundant ion, which here is *m*/*e* = 64. The isotopic distribution of TiO^+, $TiOH^+$, and $SiCl^+$ are included as reference. It can be seen that for Mo-only catalyst the ion distribution could be obtained by the convolution of TiO^+ and $TiOH^+$ mass fragments, which commonly coexist for a titania oxide sample. For the chlorine-containing catalyst, however, the ion distribution pattern is very different from the Mo-only catalyst with the *m*/*e* = 63 abundance being out of proportion. It is clear that the coexistence of TiO^+ and $TiOH^+$ mass fragments solely could not result in the observed pattern. It has been shown that chlorine can interact with silica through silanol groups for chlorine-modified silica glass;[61,68] therefore the existence of $SiCl^+$ mass fragment with its most abundant ion at *m*/*e* = 63 can explain the observed pattern over the chlorine-containing catalyst. This observation is significant in showing Si−Cl bonding on the surface. Within the detection limit of the SIMS technique, it can be concluded that chlorine interacts with silica by either replacing the surface OH groups of silanol species (SiOH) or replacing titania in Si−O−Ti groups and results in more electronegative silica−O ligands, which may be more reactive toward surface molybdena species. Consequently, molybdena species may interact preferentially with silica over titania and titania segregates from Si:Ti network to form the anatase phase.

Reaction Experiments of Oxidative Dehydrogenation of Ethane. Catalysts with Cl/Mo ratios ranging from 0 to 2 were tested for the ethane ODH reaction using 100 m^2 of equal surface area in the reactor and at temperatures of 550 and 600 °C. The turnover frequencies (TOF) for ethylene formation are presented in Table 5. At both temperature levels tested, addition of Cl clearly provides a promotional effect. This effect becomes more pronounced at higher loading levels of Cl. It should be noted

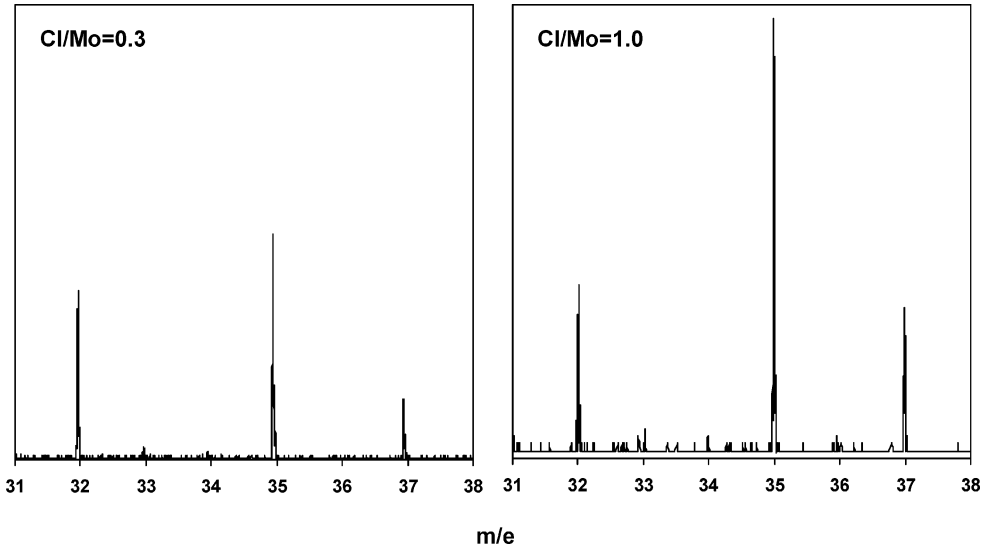

Figure 7. Negative SIMS mass spectra for (Cl/Mo)/Si:Ti catalysts.

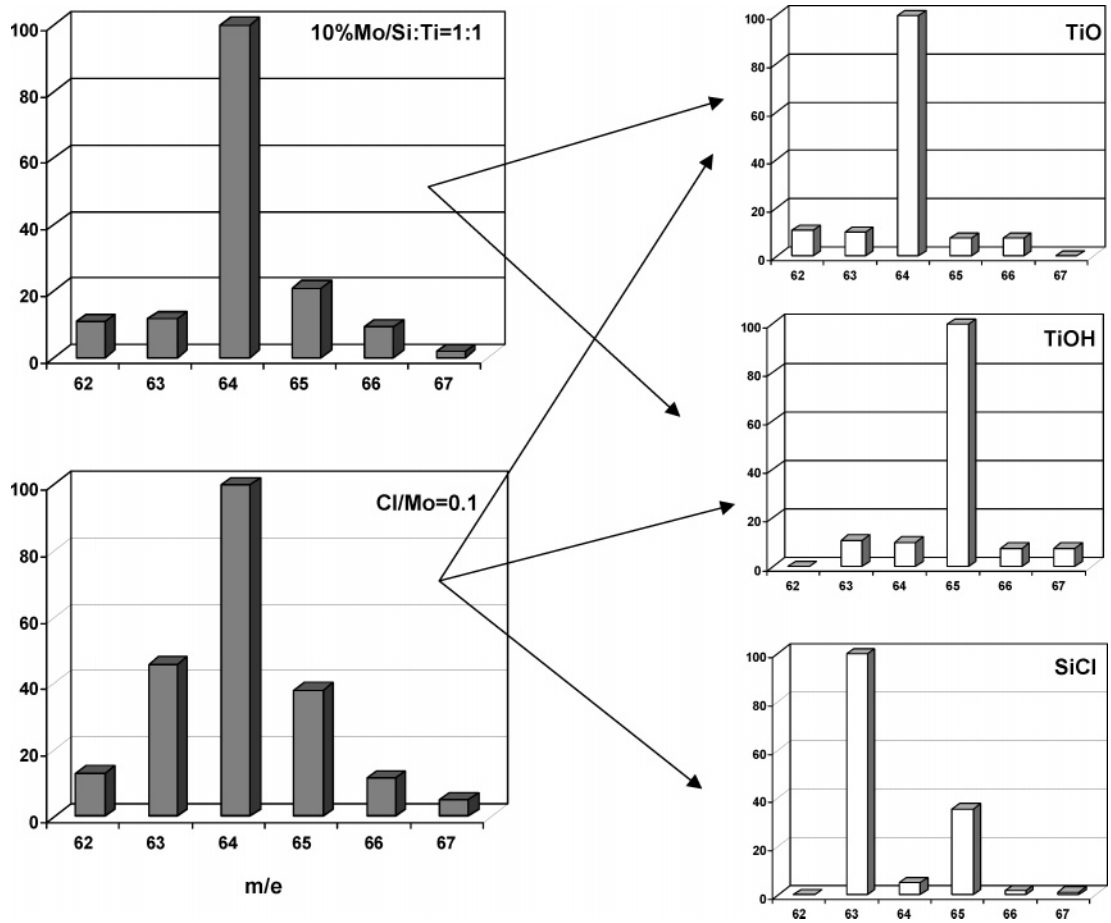

Figure 8. Positive SIMS isotopic patterns for (Cl/Mo)/Si:Ti catalysts and reference isotope patterns.

TABLE 5: Ethylene Formation Turnover Frequency

	TOF (10^{-4} s^{-1})	
catalyst	550 °C	600 °C
10% Mo/Si:Ti = 1:1	1.7	2.4
Cl/Mo = 0.1	1.9	2.6
Cl/Mo = 0.3	2.8	3.8
Cl/Mo = 1.0	3.0	3.9
Cl/Mo = 2.0	3.7	4.5

that the TOF data reported may not be the absolute values. Although the characterization results, especially Raman spectroscopy data, rule out the possibility of three-dimensional molybdenum oxide structures on the surface, we may still have Mo atoms not exposed to reaction media since "one-pot" sol−gel synthesis techniques allow dispersion of Mo throughout the entire support matrix, and not just the surface. Therefore, when TOF values are calculated by normalizing the formation rate with respect to the total number of Mo atoms, there is likely to be an error introduced since the number of active sites on the surface is smaller than the total number of Mo atoms. However, as seen through the XPS analysis, the surface concentration of Mo does not deviate significantly from the bulk concentration. Therefore, although the TOF data may not represent the true

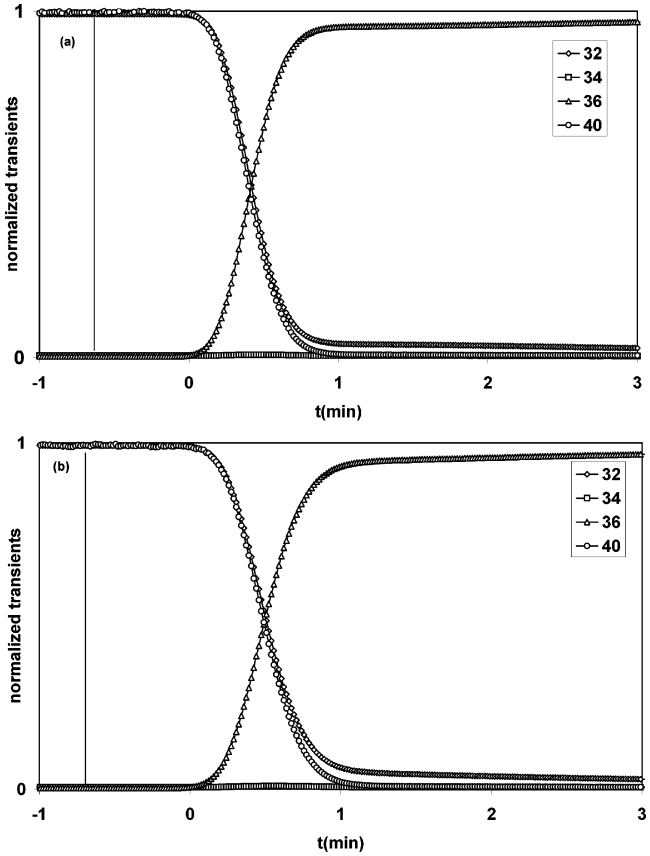

Figure 9. Isotopic oxygen switch without reaction (10% $^{16}O_2$/1% Ar/He to 10% $^{18}O_2$/He): (a) 10% Mo/Si:Ti = 1:1; (b) Cl/Mo = 1.

TOF values, the trend they exhibit is not affected. In fact, a small decrease in the surface concentration of Mo seen at the highest Cl loading levels suggests that if it were possible to determine the true number of surface sites, the promotional effect of Cl would have even been more pronounced. More extensive reaction results are presented elsewhere.[36]

Steady-State Isotopic Transient Kinetic Analysis (SSITKA). To further probe the surface residence time of different species and the involvement of lattice oxygen in the oxidation reaction pathway, steady-state isotopic transient kinetic analysis experiments were performed over 10% Mo/Si:Ti = 1:1 and Cl/Mo = 1 catalysts using $^{18}O_2$.

Figure 9 presents the transient curves of different oxygen isotopes obtained when a stream of $^{16}O_2$, Ar, and He was switched to a stream of $^{18}O_2$ and He. As can be seen in the figure, the transient curves for the two catalysts are very similar. There is essentially no cross-labeled oxygen (m/e = 34) formed following the switch. It is also noted that the $^{16}O_2$ transient relaxes to zero at almost the same rate that Ar transient does, showing a very small delay. These observations show that there is very little oxygen exchange with the surface in the absence of reducing medium, i.e., a hydrocarbon. On metal oxides, oxygen may be exchanged by two mechanisms, depending on whether oxygen exchanges one or both of its atoms with the surface of catalyst.[69−71] The results shown here indicate that the limited amount of exchange that takes place involves molecular oxygen as opposed to dissociated oxygen.

Figure 10 shows the transients for water isotopes ($H_2{}^{16}O$, $H_2{}^{18}O$) obtained when the feed stream during steady-state reaction of ethane ODH was switched from $^{16}O_2$, C_2H_6, Ar, and He to $^{18}O_2$, C_2H_6, and He over the Mo/Si:Ti catalyst. Ar transient is also included to show how long it takes for the gas-phase

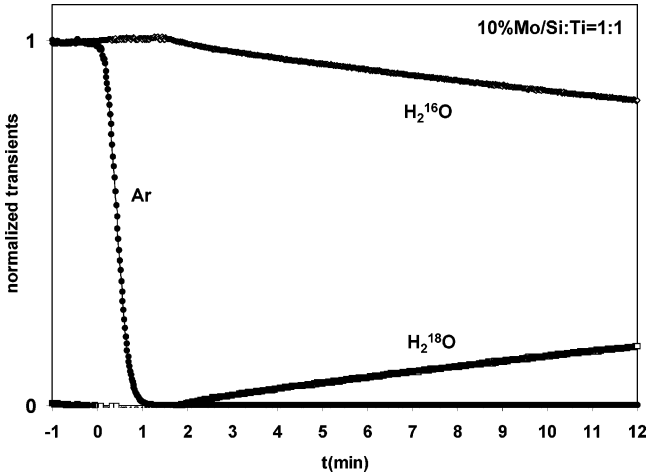

Figure 10. Oxygen isotopic switch in the presence of reaction: water isotope transients (5% ethane, 2.5% $^{16}O_2$, 1% Ar, 91.5% He to 5% ethane, 2.5% $^{18}O_2$, 92.5% He).

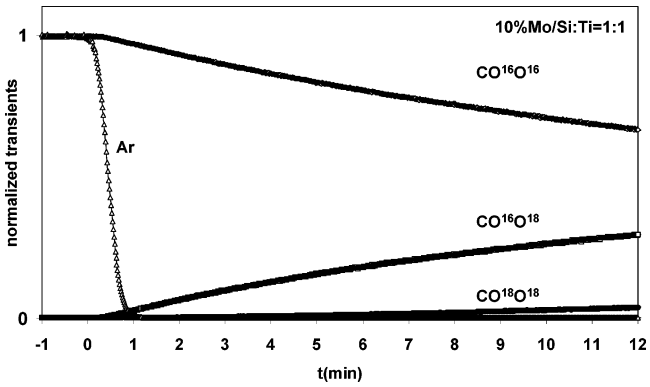

Figure 11. Oxygen isotopic switch in the presence of reaction: carbon dioxide isotope transients (5% ethane, 2.5% $^{16}O_2$, 1% Ar, 91.5% He to 5% ethane, 2.5% $^{18}O_2$, 92.5% He).

species to exit the system if there is no interaction with the surface. The ^{16}O-containing water transient is seen to stay at a very high level throughout the duration of the experiment, indicating that oxygen inserted into water primarily comes from the catalyst lattice as opposed to from the gas phase. The transients obtained over the Cl-modified catalysts (not shown) were similar. This is very different from the relaxation behavior of unlabeled oxygen we observed in the absence of reaction, indicating that only when the surface is partially reduced and oxygen vacancies are created does the lattice oxygen mobility become significant.

Figure 11 shows the transients for carbon dioxide isotopes ($C^{16}O_2$, $C^{16}O^{18}O$, and $C^{18}O_2$) obtained during the same switch. For both Mo-only and Cl-doped (not shown here) catalysts, the ^{16}O-containing carbon dioxide is seen to be the dominant isotope during the entire 12 min after the switch, indicating that, similar to water, most of the oxygen inserted into carbon dioxide comes from the catalyst lattice. Interestingly, when we compare the percentage of ^{16}O in water to that in carbon dioxide, we see that the percentages are around 82%. This suggests that the water and CO_2 formation may involve common mechanistic steps and use the same oxygen sources.

Although the slow relaxation of unlabeled isotopes could also be due to strong adsorption of the species on the surface, it is not likely to be the case here. Control experiments performed using ^{13}C-labeled ethane have shown that unlabeled CO_2 isotopes relaxed within the same time frame as Ar, indicating that CO_2 does not reside on the surface for any appreciable

length of time after it is formed. Oxygen exchange with the surface after the molecule (CO_2 or H_2O) is formed is another possibility. However, it is also unlikely since we have seen essentially no exchange of molecular oxygen with the surface in the absence of a reaction.

Conclusions

The effect of chlorine on the surface and structural characteristics of Mo/Si:Ti catalysts and their catalytic performance for oxidative dehydrogenation of ethane were examined. Cl-modified catalysts showed a significant increase in ethylene yield, mostly through improved selectivity.

In addition to the improved selectivity toward olefin formation with Cl addition, there were significant changes observed in the surface and structural characteristics of the catalysts. As seen through Raman spectroscopy and XPS analysis, with increased Cl loading, interaction of Mo═O species with Si−O ligands increased at the expense of their interaction with titania surfaces. Segregation of anatase titania was also observed, leading to an increase of Si on the surface at the expense of titania. XPS data also showed that, without forming molybdenum chloride, chlorine could significantly alter the electronic structure of molybdena species and oxygen environment around the Mo and Si species in the Si:Ti matrix. SIMS analysis provided evidence of Si−Cl bonding, which could contribute to increased connectivity between Mo and Si species. The molybdena species sharing more complex ligands with both silica and titania with indirect participation of chlorine could be responsible for the improved catalytic performance.

Isotopic labeling experiments performed using $^{18}O_2$ showed very little oxygen exchange with the surface in the absence of a reaction medium. During steady-state ethane ODH reaction, however, oxygen inserted in water and carbon dioxide molecules were found to come primarily from the catalyst lattice. Lattice oxygen involvement in the formation of water and CO_2 was very similar.

Acknowledgment. Financial support provided by the National Science Foundation (Grant CTS-9412544) is gratefully acknowledged. The authors also thank Professor Leonard Brillson and Dr. Stephen Goss for making the SIMS analysis possible.

References and Notes

(1) Kung, H. H. *Adv. Catal.* **1994**, *40*, 1.
(2) Cavani, F.; Trifiro, F. *Catal. Today* **1995**, *24*, 307.
(3) Mamedov, E. A.; Cortes-Corberan, V. *Appl. Catal.* **1995**, *127*, 1.
(4) Blasko, T.; Lopez Nieto, J. M. *Appl. Catal. A* **1997**, *157*, 117.
(5) Baerns, M.; Buyevskaya, O. *Catal. Today* **1998**, *45*, 13.
(6) Cavani, F.; Koutyrev, M.; Trifiro, F. *Catal. Today* **1996**, *28*, 139.
(7) Banares, M. A. *Catal. Today* **1999**, *51*, 319.
(8) Grubert, G.; Kondratenko, E.; Kolf, S.; Baerns, M.; Geem, P.; Parton, R. *Catal. Today* **2003**, *81*, 337.
(9) Khodakov, A.; Olthof, B.; Bell, A. T.; Iglesia, E. *J. Catal.* **1999**, *181*, 205.
(10) Chen, K.; Khodakov, A.; Yang, J.; Bell, A. T.; Iglesia, E. *J. Catal.* **1999**, *186*, 325.
(11) Chen, K.; Xie, S.; Iglesia, E.; Bell, A. T. *J. Catal.* **2000**, *189*, 421.
(12) Chen, K.; Xie, S.; Iglesia, E.; Bell, A. T. *J. Catal.* **2000**, *198*, 232.
(13) Hodnet, B. K. *Heterogeneous Catalytic Oxidation*; Wiley: New York, 2000.
(14) Finocchio, E.; Busca, G.; Lorenzelli, V.; Willey, R. J. *J. Catal.* **1995**, *151*, 204.
(15) Baldi, M.; Escribano, V. S.; Amores, J. M. G.; Milella, F.; Busca, G. *Appl. Catal.* **1998**, *17*, L175.
(16) Baldi, M.; Milella, F.; Ramis, G.; Escribano, V. S.; Busca, G. *Appl. Catal.* **1998**, *166*, 75.
(17) Busca, G.; Finocchio, E.; Lorenzelli, V.; Ramis, G.; Baldi, M. *Catal. Today* **1999**, *49*, 453.
(18) Ermini, V.; Finocchio, E.; Sechi, S.; Busca, G.; Rossini, S. *Appl. Catal.* **2000**, *190*, 157.
(19) Ermini, V.; Finocchio, E.; Sechi, S.; Busca, G.; Rossini, S. *Appl. Catal.* **2000**, *198*, 67.
(20) Busca, G. *Catal. Today* **1996**, *27*, 457.
(21) Buyevskaya, O. V.; Baerns, M. *Catal. Today* **1998**, *42*, 315.
(22) Zanthoff, H. W.; Buchholz, S. A.; Pantazidis, A.; Mirodatos, C. *Chem. Eng. Sci.* **1999**, *54*, 4397.
(23) Pantazidis, A.; Auroux, A.; Herrmann, J. M.; Mirodatos, C. *Catal. Today* **1996**, *32*, 81.
(24) Bettahar, M. M.; Costentin, G.; Savary, L.; Lavalley, J. C. *Appl. Catal.* **1996**, *145*, 1.
(25) Schlogl, R.; Knop-Gericke, A.; Havecker, M.; Wild, U.; Frickel, D.; Ressler, T.; Jentoft, R. E.; Wienhold, J.; Mestl, G.; Blume, A.; Timpe, O.; Uchida, Y. *Top. Catal.* **2001**, *15*, 219.
(26) Watson, R. B.; Ozkan, U. S. *J. Catal.* **2000**, *191*, 12.
(27) Watson, R. B.; Ozkan, U. S. *J. Catal.* **2002**, *208*, 124.
(28) Watson, R. B.; Ozkan, U. S. *J. Phys. Chem.* **2002**, *106*, 6930.
(29) Watson, R. B.; Ozkan, U. S. *J. Mol. Catal.* **2003,** *194*, 115.
(30) Watson, R. B.; Ozkan, U. S. *J. Mol. Catal.* **2004**, *208*, 233.
(31) Wang, D.; Roybek, M. P.; Lunsford, J. H. *J. Catal.* **1995**, *151*, 155.
(32) Traxel, B. E.; Hohn, K. L. *J. Catal.* **2002**, *212*, 46.
(33) Ueda, W.; Lin, S. W.; Tohmoto, I. *Catal. Lett.* **1997**, *44*, 241.
(34) Wang, S.; Murata, K.; Hayakawa, T.; Hamakawa, S.; Suzuki, K. *Energy Fuels* **2000**, *14*, 899.
(35) Dai, H. X.; Au, C. T.; Chan, Y.; Hui, K. C.; Leung, Y. L. *Appl. Catal.* **2001**, *213*, 91.
(36) Liu, C.; Ozkan, U. S. *J. Mol. Catal.* **2004**, *220*, 53.
(37) U.S. Patent 6,521,808, 2003.
(38) Ozkan, U. S.; Cai, Y.; Kumthekar, M. W.; Zhang, L. *J. Catal.* **1993**, *142*, 182.
(39) Izutsu, H.; Nair, P. K.; Maeda, K.; Kiyozumi, Y.; Mizukami, F. *Mater. Res. Bull.* **1997**, *32*, 1303.
(40) Kim, K. S.; Barteau, M. A.; Farneth, W. E. *Langmuir* **1988**, *4*, 533.
(41) Biaglow, A. I.; Gorte, R. J.; Srinivasan, S.; Datye, A. K. *Catal. Lett.* **1992**, *13*, 313.
(42) Gorte, R. J. *Catal. Today* **1996**, *28*, 405.
(43) Davis, R. J.; Liu, Z. *Chem. Mater.* **1997**, *9*, 2311.
(44) Swain, J. E.; Juskelis, M. V.; Slanga, J. P.; Miller, J. G.; Uberoi, M.; Spencer, N. D. *Appl. Catal.* **1996**, *139*, 175.
(45) Chen, K.; Bell, A. T.; Iglesia, E. *J. Phys. Chem.* **2000**, *104*, 1292.
(46) Notari, B. *Adv. Catal.* **1996**, *41*, 253.
(47) Weckhuysen, B. M.; Jehng, J. M.; Wachs, I. E. *J. Phys. Chem.* **2000**, *104*, 7382.
(48) Gao, X.; Bare, S. R.; Fierro, J. L. G.; Banarez, M. J.; Wachs. I. E. *J. Phys. Chem.* **1998**, *102*, 5653.
(49) Gao, X.; Bare, S. R.; Fierro, J. L. G.; Weckhuysen, B. M.; Wachs, I. E. *J. Phys. Chem.* **1998**, *102*, 10482.
(50) Armaroli, T.; Milella, F.; Notari, B.; Willey, R. J.; Busca, G. *Top. Catal.* **2001**, *15*, 63.
(51) Jehng, J. M.; Hu, H.; Gao, X.; Wachs, I. E. *Catal. Today* **1996**, *28*, 335.
(52) Wachs, I. E. *Catal. Today* **1996**, *27*, 437.
(53) Banares, M. A.; Hu, H.; Wachs, I. E. *J. Catal.* **1994**, *150*, 407.
(54) Gao, X.; Wachs, I. E. *J. Catal.* **2000**, *192*, 18.
(55) Briggs, D.; Seah, M. P. *Practical Surface Analysis*, 2nd ed.; Wiley: New York, 1993.
(56) Grim, S. O.; Matienzo, L. J. *Inorg. Chem.* **1975**, *14*, 1014.
(57) Beccaria, A. M.; Poggi, G.; Castello, G. *Br. Corros. J.* **1995**, *30*, 283.
(58) Orita, M.; Kojima, I.; Iyazaki, E. *Bull. Chem. Soc. Jpn.* **1986**, *59*, 689.
(59) Portela, L.; Grange, P.; Delmon, B. *J. Catal.* **1995**, *156*, 243.
(60) Nagai, M.; Goto, Y.; Ishii, H.; Omi, S. *Appl. Catal.* **2000**, *192*, 199.
(61) Chmel, A.; Svetlov, V. N. *Opt. Mater.* **1995**, *4*, 729.
(62) Chmel, A.; Svetlov, V. N. *J. Non-Cryst. Solids* **1996**, *195*, 176.
(63) Stakheev, A. Y.; Shpiro, E. S.; Apijok, J. *J. Phys. Chem.* **1993**, *97*, 5668.
(64) Adriaens, A.; Vaeck, L. V.; Adams, F. *Mass Spectrom. Rev.* **1999**, *18*, 48.
(65) Vickerman, J. C.; Oakes, A.; Gamble, H. *Surf. Interface Anal.* **2000**, *29*, 349.
(66) Borg, H. J.; van den Oetelaar, L. C. A.; Niemantsverdriet, J. W. *Catal. Lett.* **1993**, *17*, 81.
(67) Zhou, Y.; Wood, M. C.; Winograd, N. *J. Catal.* **1994**, *146*, 82.
(68) Sartre, A.; Dazord, J.; Bouix, J. *J. Opt.* **1984**, *15*, 302.
(69) Smith, M. R.; Ozkan, U. S. *J. Catal.* **1993**, *142*, 226.
(70) Driscoll, S. A.; Ozkan, U. S. *J. Phys. Chem.* **1993**, *97*, 11524.
(71) Winter, E. R. S. *J. Chem. Soc., Ser. A* **1969**, *23*, 2889.